Forced Frequency Response Analysis of a Gudgeon Pin

Ekrem Gülsevinçler[1*]

[1*] Sinop University, Faculty of Engineering and Architecture, Departmant of Nuclear Energy Engineering, Sinop, Turkey, (ORCID: 0000-0002-4787-6275), egulsevincler@sinop.edu.tr

Abstract

In this study, forced frequency response analysis was applied on the gudgeon pin. Ansys Mechanical 19.2 program was used to analyze the vibration on the gudgeon pin. Once completed in the finite element analysis, a note from the modal results, the model's natural frequencies range from 38721 to 79346 Hertz for the first 12 modes. According to the modal analysis results, the gudgeon pin will not be subjected to resonance during working. Therefore, a frequency scan including modal analysis is required to detect resonant frequencies that may coincide with the natural frequencies of the first 12 modes obtained in modal analysis. Consequently, harmonic analysis has been solved using the mode superposition method with 50 intervals with 1000 Hz steps in the range of 30000-80000 Hz. To dampen the resonant frequencies, harmonic analyzes were repeated using six different constant damping ratios, and the results were compared.

Keywords: Gudgeon Pin, Forced Frequency Response Analysis, Harmonic Analysis, Resonance

Piston Pimi Zorlanmış Frekans Yanıt Analizi

Öz

Bu çalışmada, piston pimi üzerinde zorlanmış frekans yanıt analizi uygulanmıştır. Piston pimindeki titreşimi analiz etmek için Ansys Mechanical 19.2 programı kullanılmıştır. Modal analiz sonuçlarına dayalı olan sonlu eleman analizi tamamlandığında, modelin doğal frekansları ilk 12 mod için 38721 ile 79346 Hertz arasında değişmektedir. Modal analiz sonuçlarına göre, piston pimi çalışma sırasında rezonansa maruz kalmayacaktır. Bu nedenle, modal analizde elde edilen ilk 12 modun doğal frekanslarıyla çakışabilecek rezonans frekanslarını tespit etmek için modal analizi içeren bir frekans taraması gereklidir. Sonuç olarak, 30000-80000 Hz aralığında 1000 Hz'lik adımlarla 50 aralıklı mod süperpozisyon yöntemi kullanılarak harmonik analizi çözdürülmüştür. Rezonans frekanslarını azaltmak için altı farklı sabit sönüm oranı kullanılarak harmonik analizler tekrarlanmış ve sonuçlar karşılaştırılmıştır.

Anahtar Kelimeler: Piston Pimi, Zorlanmış Frekans Yanıt Analizi, Harmonik Analiz, Rezonans

* Corresponding Author: egulsevincler@sinop.edu.tr

1. Introduction

Forced frequency response analysis an essential branch of linear dynamics. As we mentioned before, linear dynamics solves the equations of motion as a frequency-domain problem instead of a time-domain problem. In our lives, many structures experience vibration or cyclic loading. Such loading conditions can usually be represented by sinusoidal loading. For example, when sitting in the car and start the engine, one can feel certain vibration levels more or less. The source of such vibration is a physics movement of the piston (Geng & Chen, 2005; Liu & Randall, 2005; Moosavian et al., 2016, 2017; Reghu et al., 2018; Wu et al., 2019) and crankshafts (Fung & Chen, 1998; Karkoub, 2000; Veciana Fontanet et al., 2021) of the vehicle's motor. Anyone see that the forcing load repeats in a sinusoidal repetition for each cylinder. The engine motor has multiple cylinders, so multiple excitations per revolution, such as cyclic movement, might be magnified depending on how well the engine vibration (Diéguez et al., 2018; Geng et al., 2003; Geng & Chen, 2005; Gosala et al., 2021; Moosavian et al., 2016, 2017; Naseri et al., 2020) isolation system or even the entire car structure is built.

One of the main goals of harmonic analysis is to avoid resonance for given excitations. Whether it is a partial resonance (Binoy et al., 2013) or a global resonance (Liao, 2014; Yao & Li, 2019), the result could be devastating to the structure. Most engineering structures will be vibration tested in the industry to verify the dynamic response expected to experience dynamic loading. Besides avoiding harmonic resonance analysis, we can also tell us the magnitude of the vibration to prevent fatigue failure. The harmonic analysis results can help an engineer understand the significance of different model designs effectively. Additionally, harmonic analysis can be used alongside physical testing, such as a shaker table with sine sweep ("Closed-Loop Random Vibration Control of a Shaker Table with a Microcomputer: M. L. Wang, Soil Dynamics & Earthquake Engineering, 13(4), 1994, Pp 259–266," 1995; Kihm & Delaux, 2013; Wang, 1994) to correlate the natural frequencies and damping models.

Frequency response analysis can be used to plot the level of vibration (displacements or accelerations) as a function of frequency. Another type of use is the fatigue account input. When combined with a PSD (Power Spectral Density) (Gharaibeh & Pitarresi, 2019; Jannoun et al., 2017; Muhammad et al., 2020; Trapp & Wolfsteiner, 2021), the structure's lifetime can be determined.

1.1. Governing Equations

The harmonic function is comprised of three main variables: Frequency, amplitude, and phase angle. For a given time t, the corresponding force can be computed.

$$F_{\dot{i}} = F_{\dot{i}} \sin(\omega_i t + \theta_i) \tag{1}$$

Where, $F_{\dot{i}}$ is amplitude, ω_i is imposed circular frequency, θ_i is phase angle and t is time. The imposed circular frequency, ω_i is a simple expression and typically has units of radians/sec.

$$\omega = 2\pi f \tag{2}$$

Where f is imposed frequency:

$$f = \frac{1}{T_f} \tag{3}$$

Where T_f is period. A harmonic force (f) is applied to the mass (m) and measuring the resulting displacement (u) and phase angle (θ) as sweep the excitation frequency from zero to three times the natural frequency. Governing equation of harmonic motion:

$$m\ddot{u} + c\dot{u} + ku = f \sin \omega t \tag{4}$$

Where u is the displacement of mass:

$$u = \frac{f/k}{\sqrt{(1-(\omega/\omega_n)^2)^2+(2\zeta\omega/\omega_n)^2}} \tag{5}$$

Where ζ is damping ratio:

$$\zeta = \frac{c}{C_c} \tag{6}$$

Where C_c is critical damping:

$$C_c = 2\sqrt{km} \tag{7}$$

If each term is divided by m in governing equation of harmonic motion:

$$\ddot{u} + \frac{c}{m}\dot{u} + \frac{k}{m}u = \frac{f}{m}\sin \omega t \tag{8}$$

When $2\zeta\omega_n$ is written instead of $\frac{c}{m}$ and ω_n^2 instead of $\frac{k}{m}$, the formula becomes as follows:

$$\ddot{u} + 2\zeta\omega_n\dot{u} + \omega_n^2 u = \frac{f}{m}\sin \omega t \tag{9}$$

Here, ω_n is the natural frequency and ω is the external/forcing/driving frequency. If the applied frequency is equal to the natural frequency, then a resonance will occur. So theoretically, if there is no damping, then infinite amplitude will occur, but damping a frequency increases a lot, even though damping it is only a finite value. If it matches, then the resonance will occur where a large amplitude. The formula becomes the following when Y is written instead of $\frac{m}{f}$.

$$\ddot{u} + 2\zeta\omega_n\dot{u} + \omega_n^2 u = \frac{1}{Y}\sin \omega t \tag{10}$$

When multiplying both sides of the equation by S:

$$S\ddot{u} + 2\zeta\omega_n S\dot{u} + \omega_n^2 Su = \sin \omega t \tag{11}$$

The total response of the harmonic system is the sum of the homogeneous solution u_{HS} and the particular solution u_{PS}.

$$u(t) = u_{HS} + u_{PS} \tag{12}$$

Where homogeneous solution, u_h would be equal to "0".

$$u_{HS} = \ddot{u} + 2\zeta\omega_n\dot{u} + \omega_n^2 u = 0 \tag{13}$$

If $0<\zeta<1$:

$$u_{HS} = e^{-\zeta\omega_n t}\left[(u\cos\omega t) + \left(\frac{\dot{u}+\zeta\omega_n u}{\omega}\right)\sin\omega t\right] \tag{14.1}$$

If $\zeta=1$:

$$u_{HS} = e^{-\zeta\omega_n t}[u(1+\omega_n t) + \dot{u}t] \tag{14.2}$$

If $\zeta>1$:

$$u_{HS} = e^{-\zeta\omega_n t}\left[u\cosh(\omega^* t) + \frac{\dot{u}+\zeta\omega_n u}{\omega^*}\sinh(\omega^* t)\right] \tag{14.3}$$

The particular solution equation is given below:

$$u_{PS} = A\sin\omega t + B\cos\omega t \tag{15.1}$$

$$\dot{u}_{PS} = A\,\omega\cos\omega t - B\,\omega\sin\omega t \tag{15.2}$$

$$\ddot{u}_{PS} = -A\,\omega^2\sin\omega t - B\,\omega^2\cos\omega t \qquad (15.3)$$

If the terms in Equation (15) are applied to Equation (11):

$$S(-A\,\omega^2\sin\omega t - B\,\omega^2\cos\omega t) + 2\zeta\omega_n S(A\,\omega\cos\omega t - B\,\omega\sin\omega t) + \omega_n^2 S(A\sin\omega t + B\cos\omega t) = \sin\omega t + 0\cos\omega t \qquad (16)$$

A and B terms are obtained from the equation as follows:

$$A = \frac{\omega_n^2 - \omega^2}{S[(\omega_n^2 - \omega^2) + (2\zeta\omega_n\omega)^2]} \qquad (17)$$

$$B = \frac{2\zeta\omega_n\omega}{S[(\omega_n^2 - \omega^2) + (2\zeta\omega_n\omega)^2]} \qquad (18)$$

The A term which obtained from Equation (17) and the B term, which obtained from Equation (18), are put in Equation (15.1), u_{PS} can be written as follows.

$$u_{PS} = \frac{\omega_n^2 - \omega^2}{S[(\omega_n^2 - \omega^2) + (2\zeta\omega_n\omega)^2]}\sin\omega t + \frac{2\zeta\omega_n\omega}{S[(\omega_n^2 - \omega^2) + (2\zeta\omega_n\omega)^2]}\cos\omega t \qquad (19)$$

The ratio of forcing frequency to natural frequency r:

$$r = \frac{\omega}{\omega_n} \qquad (20)$$

When Equation (20) is substituted on Equation (19), the equation becomes:

$$u_{PS} = \frac{(1-r^2)f/k}{[(1-r^2)^2 + (2r\zeta)^2]}\sin\omega t + \frac{(-2r\zeta)f/k}{[(1-r^2)^2 + (2r\zeta)^2]}\cos\omega t \qquad (21)$$

If Equation (12), Equation (14), and Equation (21) are taken together, the total response of the harmonic system is expressed as follows:

If $0 < \zeta < 1$:

$$u(t) = e^{-\zeta\omega_n t}\left[(u\cos\omega t) + \left(\frac{\dot{u} + \zeta\omega_n u}{\omega}\right)\sin\omega t\right] + \frac{(1-r^2)f/k}{[(1-r^2)^2 + (2r\zeta)^2]}\sin\omega t + \frac{(-2r\zeta)f/k}{[(1-r^2)^2 + (2r\zeta)^2]}\cos\omega t \qquad (22.1)$$

If $\zeta = 1$:

$$u(t) = e^{-\zeta\omega_n t}[u(1 + \omega_n t) + \dot{u}t] + \frac{(1-r^2)f/k}{[(1-r^2)^2 + (2r\zeta)^2]}\sin\omega t + \frac{(-2r\zeta)f/k}{[(1-r^2)^2 + (2r\zeta)^2]}\cos\omega t \qquad (22.2)$$

If $\zeta > 1$:

$$u(t) = e^{-\zeta\omega_n t}\left[u\cosh(\omega^* t) + \frac{\dot{u} + \zeta\omega_n u}{\omega^*}\sinh(\omega^* t)\right] + \frac{(1-r^2)f/k}{[(1-r^2)^2 + (2r\zeta)^2]}\sin\omega t + \frac{(-2r\zeta)f/k}{[(1-r^2)^2 + (2r\zeta)^2]}\cos\omega t \qquad (22.3)$$

2. Material and Method

2.1. Gudgeon Pin

The gudgeon pin articulates the piston and the piston rod. It transfers the combustion end pressure acting on the piston to the connecting rod. Piston pins are usually made hollow to keep them light. However, forces are occurring due to combustion; It forces the pin to bend, oval deformation, and shear in significant cross-sections (Strozzi et al., 2018).

Chrome-nickel alloy cementation steels and nitride steels are used for the pin to work under challenging conditions (gudgeon pins can withstand high pressure and impacts caused by combustion). The gudgeon pin included in this paper researched was made of AISI 8550 quality nitration steel. It is

pre-hardened (27-33 HRC) steel containing aluminum and has higher nitration ability due to its aluminum content. AISI 8550 quality nitration steel can be used in screws and barrels of plastic extrusion machines, shafts of all kinds, machine parts, gear manufacturing, and plastic injection molds. The mechanical properties of AISI 8550 nitration steel are given in Table 1. In addition, the technical drawing and FEA analysis boundary conditions of the gudgeon pin are given in Fig. 1.

Table 1. Mechanical properties of AISI 8550 nitration steel

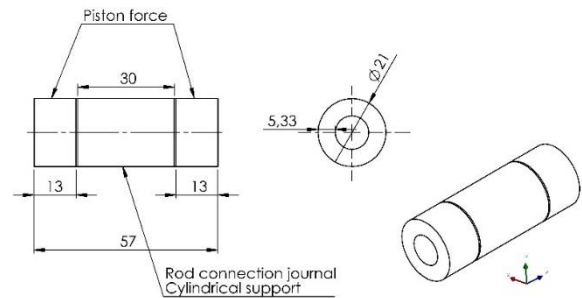|	
Density ($\times 1000$ kg/m^3)	7.7-8.03
Poisson's Ratio	0.28
Elastic Modulus (GPa)	205
Tensile Strength (Mpa)	1050
Yield Strength (Mpa)	640
Elongation (%)	11
Hardness (HV)	950

Fig. 1. The technical drawing and FEA analysis boundary conditions of the gudgeon pin

Gudgeon pins are damaged due to fatigue due to harmonic and random vibrations during long cycles (Xu & Yu, 2010; Yu et al., 2007). Therefore, in addition to the modal analysis of the model, a frequency sweep with harmonic analysis should be performed, and resonant frequencies should be determined to prevent this damage or extend the fatigue life.

2.2. Gudgeon Pin Phase Angle

Two or four-cylinder, two or four-stroke internal combustion engines are considered; The piston in a cylinder will be exposed to a force in the (-) y-direction at phase angle 0º due to the combustion effect. On the other hand, while the piston reaches the upper dead point on the cylinder, it will be exposed to a force in the (+) y-direction at phase angle 180º (Fig. 2) (Haftirman, 2016). The gudgeon pin, connected to the piston, will be exposed to a force in the (+) y and (-) y-directions at 0º and 180º phase angles.
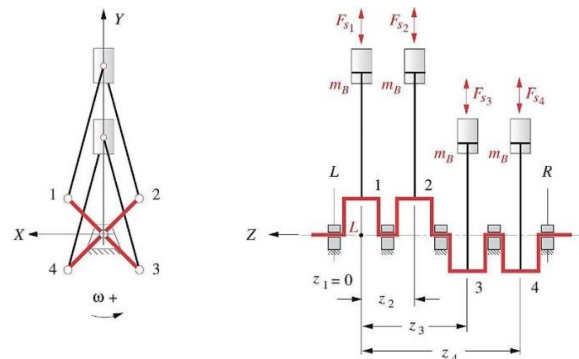

Fig. 2. Gudgeon pin phase angle for the crank position (Haftirman, 2016)

2.3. Finite Element Analysis of The Gudgeon Pin

Finite element analysis (FEA) is used to analyze the vibration on the piston pin, and Ansys Mechanical 19.2 program was used as a finite element analysis program. The natural frequencies of the piston pin should be considered to prevent the damage that may be caused by the vibration inside the engine on the piston pin. Therefore, a harmonic analysis frequency scan should be performed in the minimum and maximum natural frequency range, and resonant frequencies that may occur should be determined.

There is a need for a modal analysis for harmonic analysis and static structural analysis for pre-stress as an input of modal analysis. The mesh required for these analyzes was knitted in Ansys Mechanical 19.2 program in a program-controlled manner. Quadratic element type is used as mesh element type. The number of mesh elements is 107,744 and the number of nodes is 474,852 (Fig. 3).
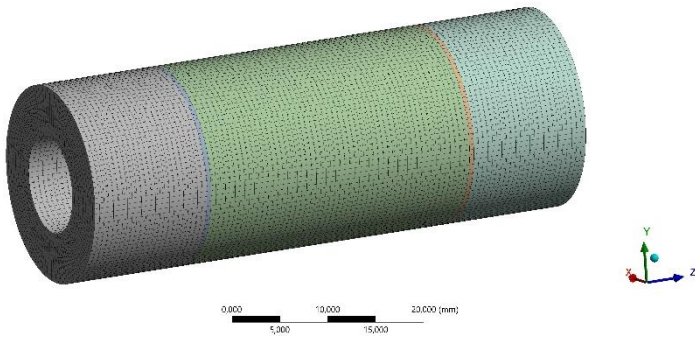

Fig. 3. Mesh topology of the gudgeon pin

In the static structural analysis, which is the first step of finite element analysis, cylindrical support at the connecting rod journal and applied force of 3275N and -y-direction in the piston connection journal is defined. In the second step, modal analysis, the stress obtained in the static structural analysis was determined as pre-stress, and the first 12 modes were analyzed. In the third step, harmonic analysis, two different forces are defined in two different phase angles in equal and opposite directions. The forces defined in the harmonic analysis are given in Table 2.

Table 2. Harmonic analysis applied force details

Force	Magnitude (N)	Direction	Phase Angle (°)
Force 1	3275N	-Y	0
Force 2	3275N	Y	180

The force on the gudgeon pin is equal to the force on the piston. The force on the piston depends on the cylinder bore diameter and cylinder pressure. For example, the force applied to the piston will be 3275N under a cylinder with a diameter of 4.46 inches at 325 kPa internal pressure.

In order to dampen the resonant frequencies, harmonic analyzes were repeated using six different constant damping ratios, and the results were compared.

$$\zeta_0 = 0 \tag{23.1}$$

$$\zeta_1 = 0.01 \tag{23.2}$$

$$\zeta_2 = 0.02 \tag{23.3}$$

$$\zeta_3 = 0.05 \tag{23.4}$$

$$\zeta_4 = 0.1 \tag{23.5}$$

$$\zeta_5 = 0.2 \tag{23.6}$$

In the harmonic analysis, a frequency scan was made in the natural frequency range obtained in the modal analysis, and the resonant frequencies were determined. Detailed information on harmonic analysis is examined in detail in the results and discussion section.

3. Results and Discussion

3.1. Static Structural Analysis Result

Gudgeon pin is subjected to shear forces between connecting rod and piston. Under the 3275N applied force, the model's Equivalent (Von-Mises) minimum stress value is 2,9934e-004 MPa, maximum stress value resulting from the static structural analysis 81,21 MPa, and average stress value is 4,6258 MPa (Fig. 4). The maximum total deformation value was calculated as 1.4599e-003 mm (Fig. 5).
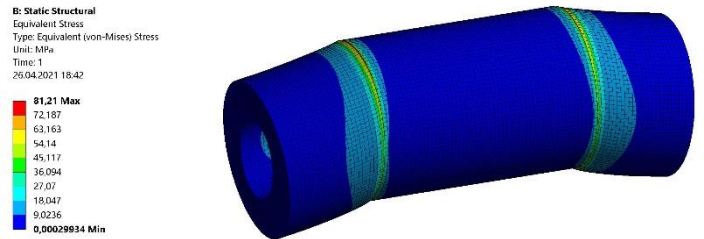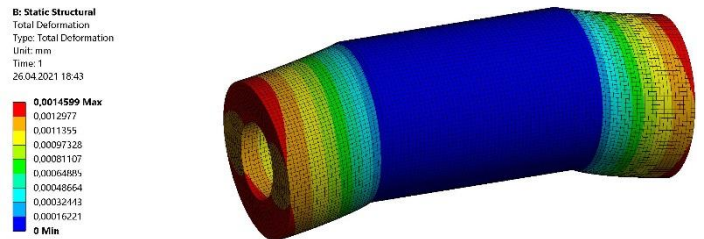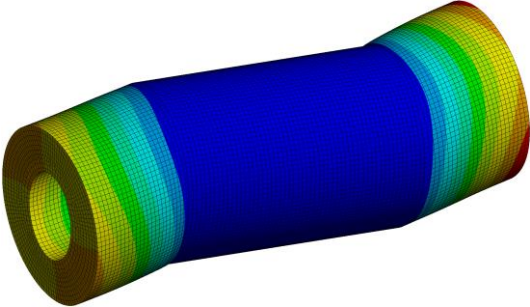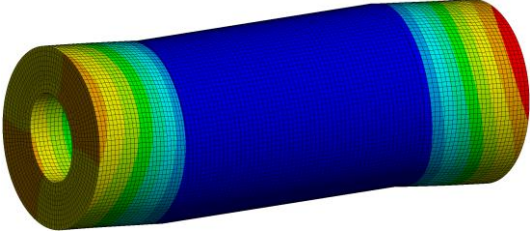

Fig. 4. Equivalent stress result
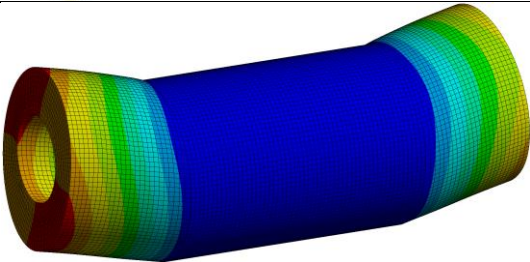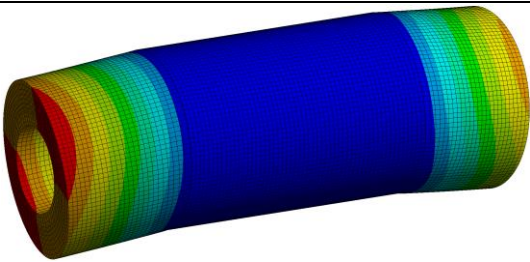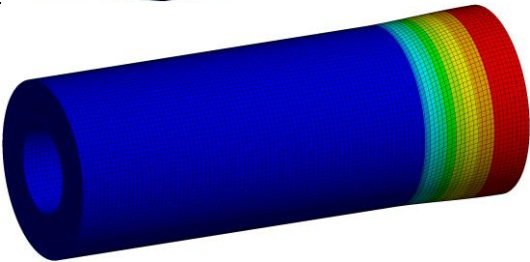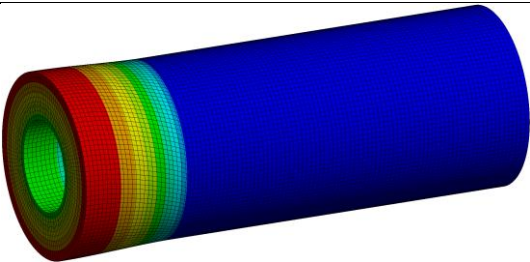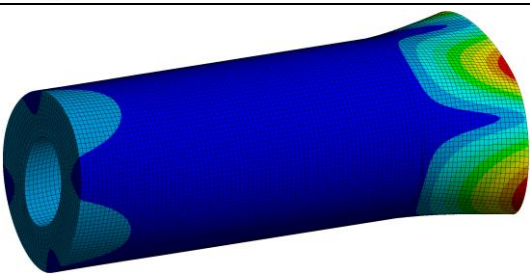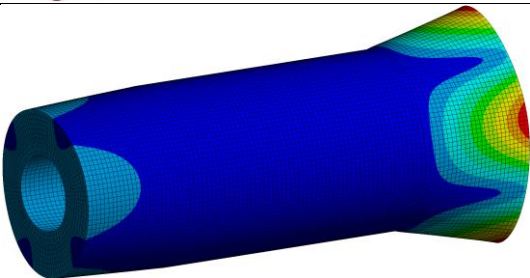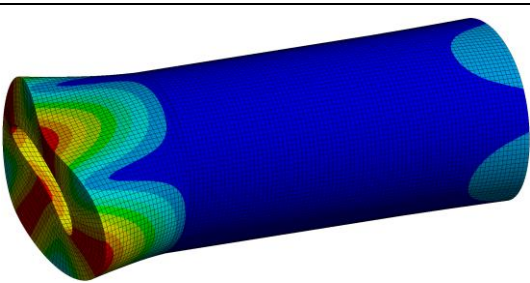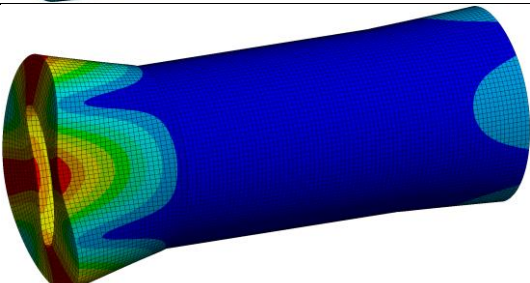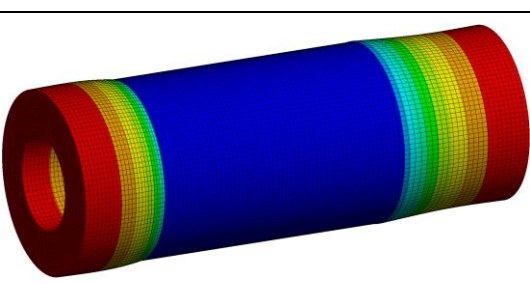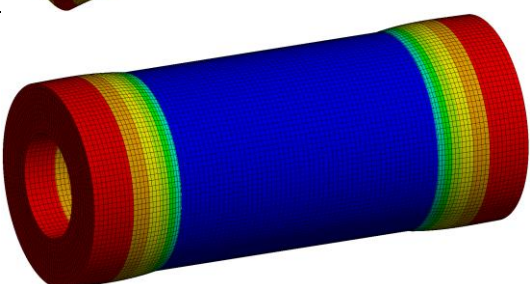
Fig. 5. Total deformation result

3.2. Modal Analysis Result

The modal analysis uses the static structural pre-stress (3275N). Once completed, a note from the modal results, the model's natural frequencies range from 38721 to 79346 Hertz for the first 12 modes. Table 3 shows the first 12 natural frequencies and main vibration directions as obtained from the modal analysis. In the first 12 modes, it was observed that every two modes have the same mode shape mirrored view.

Table 3. Modal analysis results for first 12 modes

Mode	Natural frequency (Hz)	Mode shape	Mode	Natural frequency (Hz)	Mode shape
Mode 1	38721		Mode 2	38721	
Mode 3	38724		Mode 4	38724	
Mode 5	53839		Mode 6	53840	
Mode 7	57846		Mode 8	57846	
Mode 9	57846		Mode 10	57846	
Mode 11	79142		Mode 12	79346	

3.3. Harmonic Analysis Result

According to the modal analysis results, the gudgeon pin will not be subjected to resonance during working. Therefore, a frequency scan including modal analysis is required to detect resonant frequencies that may coincide with the natural frequencies of the first 12 modes obtained in modal analysis.

(a)

(b)

(c)

Fig. 6. Frequency response normal stress amplitude a) x-axis b) y-axis c) z-axis

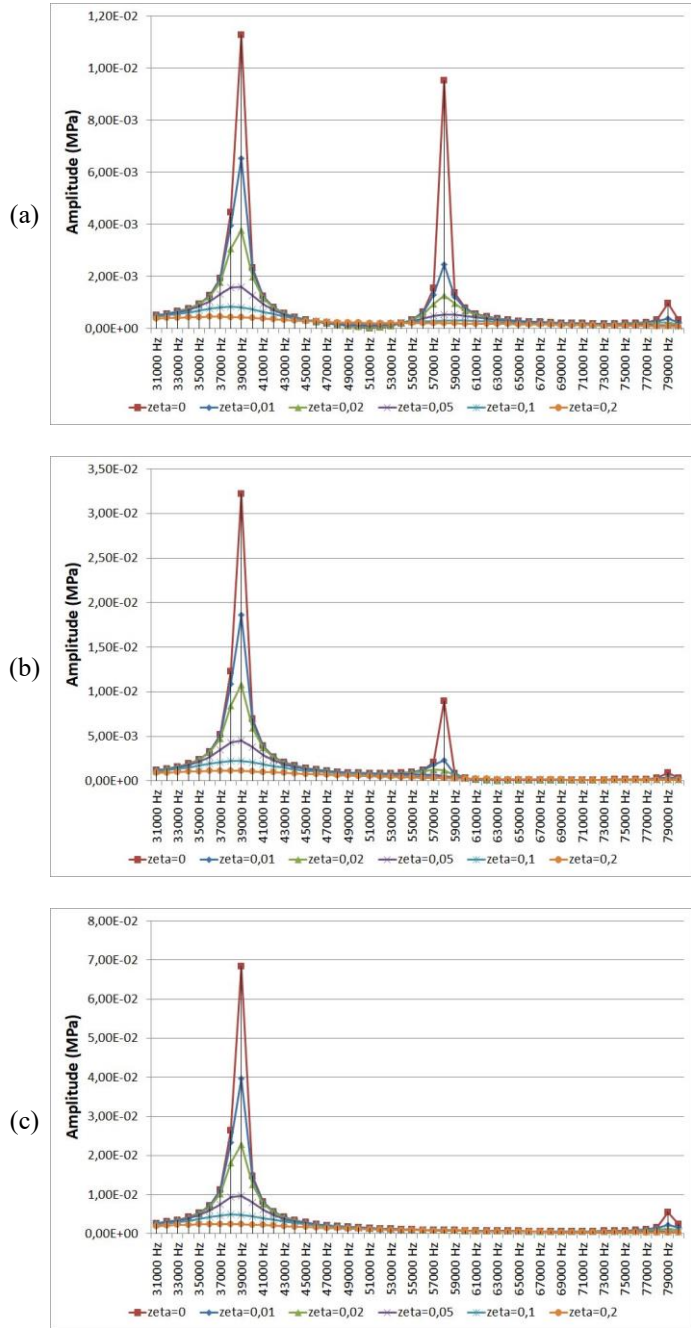For this reason, harmonic analysis has been solved by using the mode superposition method with 50 intervals with 1000 Hz steps in the range of 30000-80000 Hz.

(a)

(b)

(c)
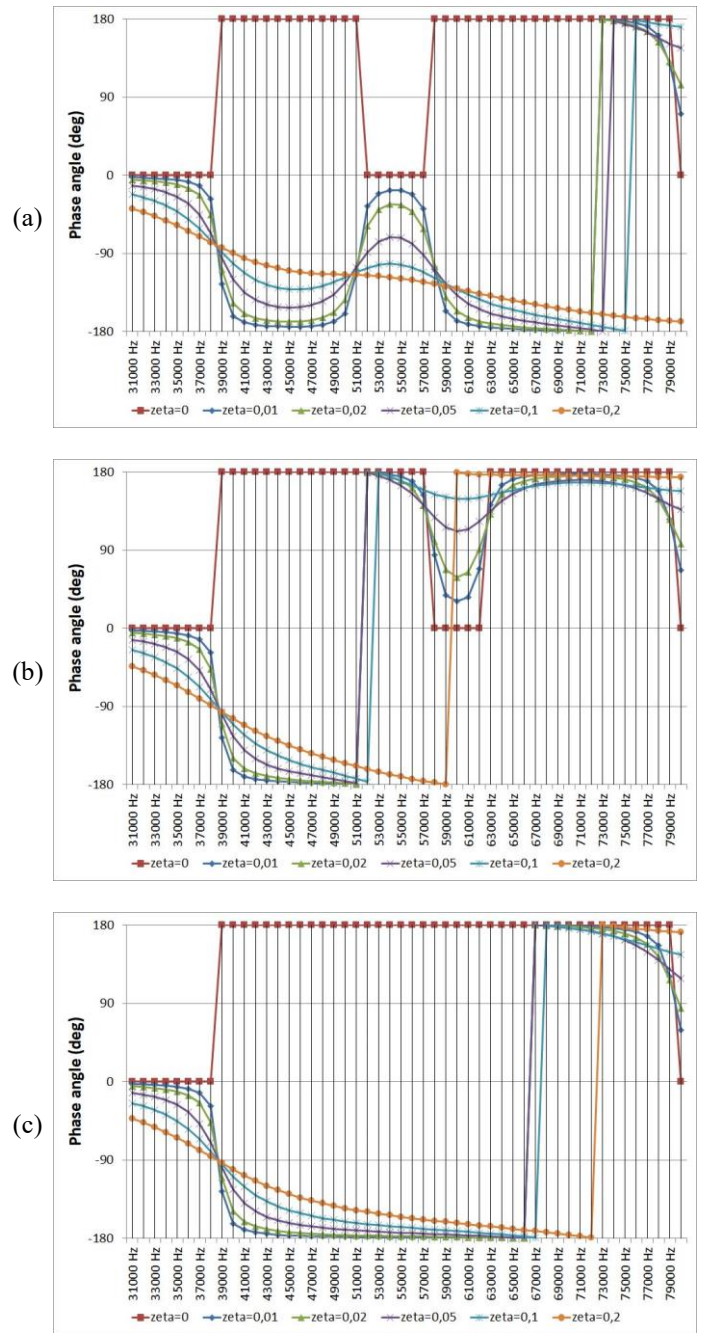
Fig. 7. Frequency response normal stress phase angle a) x-axis b) y-axis c) z-axis

According to the frequency response normal stress x-axis amplitude results (Fig. 6a), three different resonant frequency values were 39000 Hz, 58000 Hz, and 79000 Hz. Frequency response occurred in normal stress x-axis at maximum amplitude 39000 Hz frequency and 180º phase angle (Fig. 7a). The 79000 Hz value has a lower resonant frequency than the others and does not significantly amplitude. As a result of the frequency response, normal stress y-axis amplitude (Fig. 6b) has the same resonant frequencies as in the x-axis. However, the resonant amplitude values of 58000Hz and 79000 Hz are significantly lower relative to the x-axis. It is also seen from the graph that the amplitude value at 39000 Hz has a value approximately three times the value on the x-axis. The y-axis frequency response occurred in the normal stress y-axis at maximum amplitude 39000 Hz frequency and 180º phase angle (Fig. 7b). Only two resonant frequencies are resulting from the frequency response

normal stress z-axis amplitude (Fig. 6c). The resonant frequency amplitude value at 39000 Hz is approximate twice the amplitude value on the y-axis. Although there is a minor resonant value at 79000 Hz, it does not have a significant amplitude value. As on the x and y-axis, frequency response occurred in normal stress y-axis at maximum amplitude 39000 Hz frequency and 180º phase angle (Fig. 7c)

value of 79000Hz was detected in the frequency response directional deformation graph on the z-axis, but it does not have a significant amplitude value.

(a)

(b)

(c)

Fig. 8. Frequency response directional deformation amplitude a) x-axis b) y-axis c) z-axis

Frequency response directional deformation in all three axes was realized at a maximum amplitude of 39000 Hz. The maximum amplitude value on the x-axis is 6.4426e-006 mm (Fig. 8a) at the phase angle is 180° (Fig. 9a), the maximum amplitude value on the y-axis is 4.886e-002 mm (Fig. 8b) at the phase angle is -9.2564e-014° (Fig. 9b), the maximum amplitude value on the z-axis is 1.8931e-009 mm (Fig. 8c) at the phase angle is -9.2649e-014° (Fig. 9c). A little resonant frequency
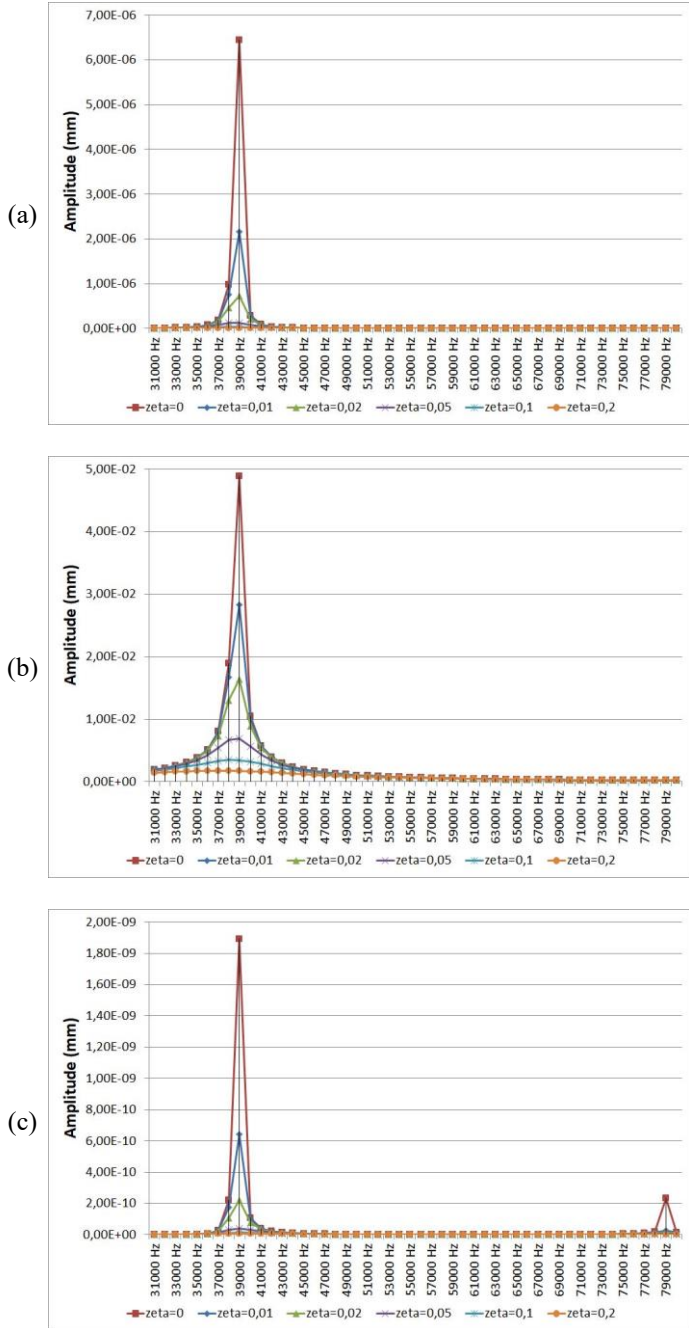

(a)

(b)

(c)

Fig. 9. Frequency response directional deformation phase angle a) x-axis b) y-axis c) z-axis

In the frequency response normal elastic strain x-axis amplitude graph, three different resonant frequency values were determined as 39000 Hz, 58000 Hz, and 79000 Hz (Fig. 10a). The resonant frequency with the highest amplitude value occurred at 39000 Hz and -9.2564e-014° phase angle (Fig. 11a). The resonant frequency of 58000 Hz is approximately two-thirds of the amplitude value occurring at 39000 Hz. The amplitude of the resonant frequency value occurring at 79000 Hz has no significant value. In the frequency response normal elastic strain y-axis amplitude plot (Fig. 10b), the highest resonant frequency occurred at 58000 Hz and -9.2564e-014° phase angle (Fig. 11b). The resonant frequency of 39000 Hz is approximately four-fifths

of the amplitude value occurring at 58000 Hz. The amplitude of the resonant frequency value occurring at 79000 Hz does not significantly value the x-axis. In the frequency response normal elastic strain z-axis amplitude plot (Fig. 10c), the highest resonant frequency occurred at 39000 Hz and 180° phase angle (Fig. 11c). A resonant frequency of 58000 Hz was not detected in the z-axis, but a low amplitude resonant frequency was detected at 79000 Hz as in the x and y axes.

(a)

(b)

(c)
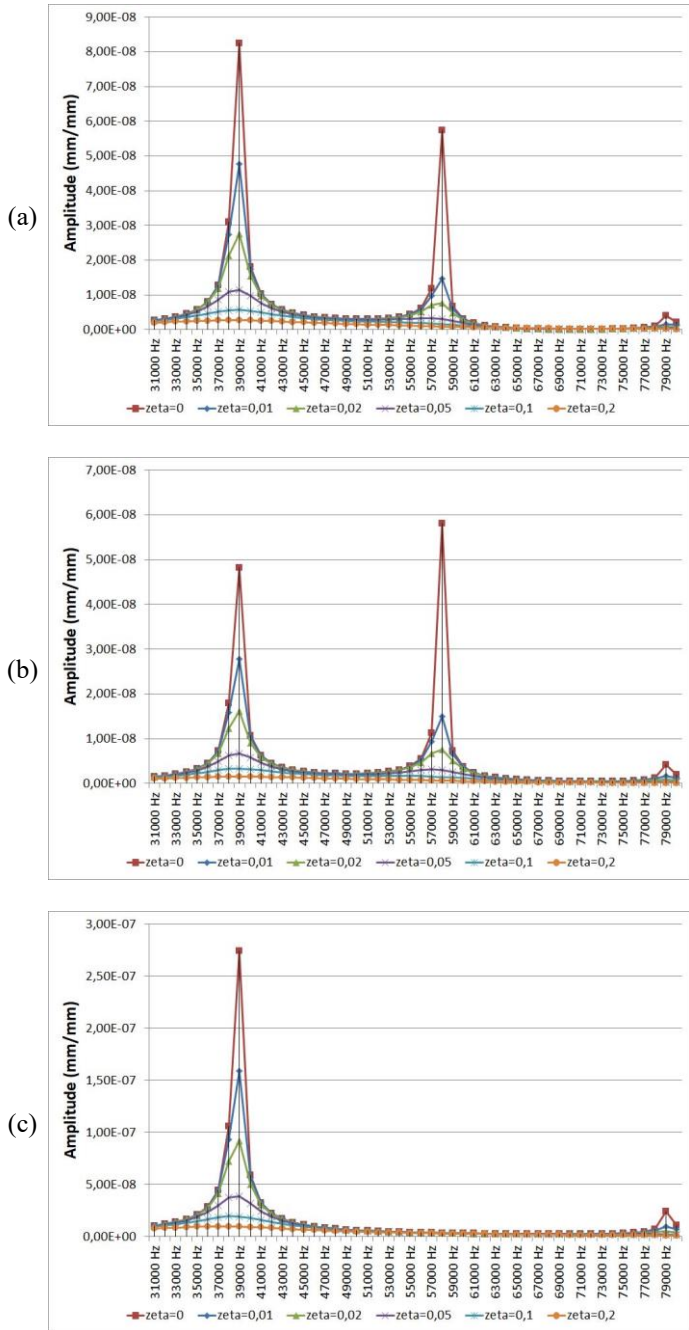
Fig. 10 Frequency response normal elastic strain amplitude a) x-axis b) y-axis c) z-axis

(a)

(b)

(c)
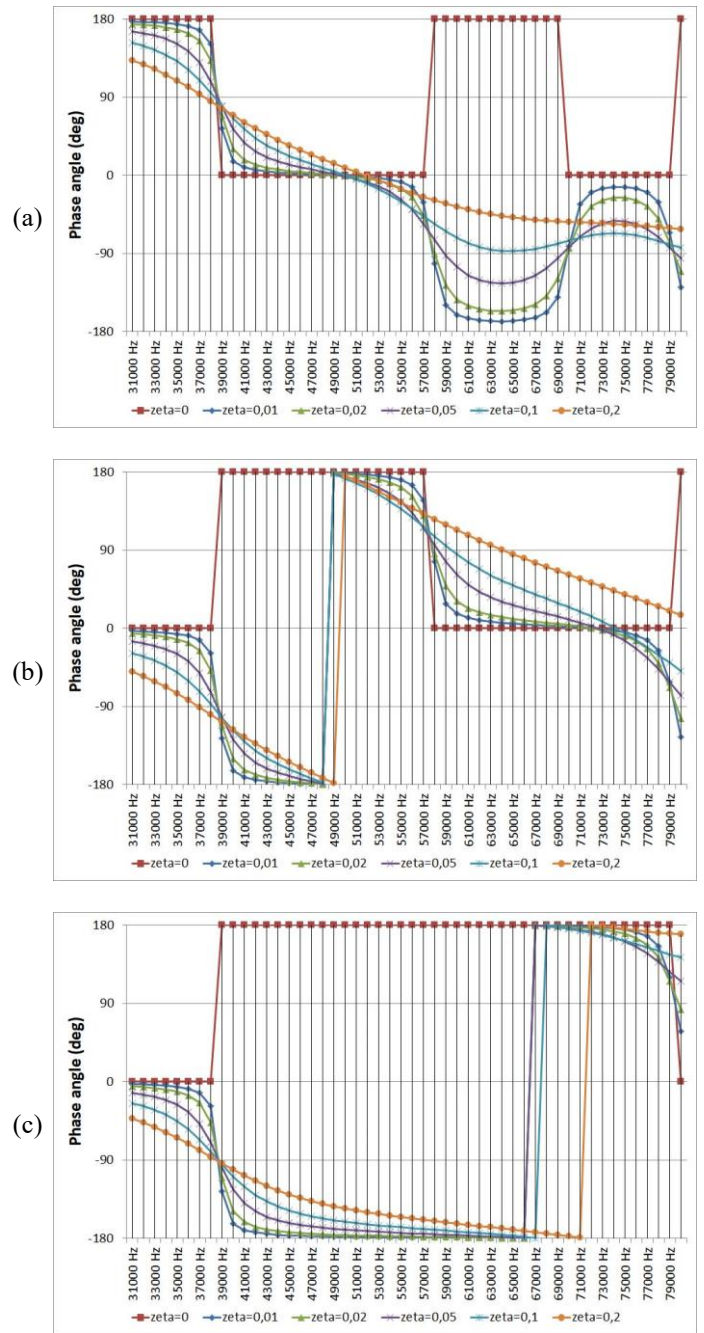
Fig. 11 Frequency response normal elastic strain phase angle a) x-axis b) y-axis c) z-axis

When the normal stress values are compared concerning the constant damping ratio ζ (Table 4), it is seen that it is 42% damping at the resonant frequency amplitude at ζ_1, 66.5% at ζ_2, 85.9% at ζ_3, 92.8% at ζ_4 and 96,3% at ζ_5.

When the directional deformation values are compared concerning the constant damping ratio ζ (Table 5), it is seen that it is 58.1% damping at the resonant frequency amplitude at ζ_1, 81.2% at ζ_2, 93.9% at ζ_3, 97.2% at ζ_4 and 98.7% at ζ_5.

When the normal stress values are compared concerning the constant damping ratio ζ (Table 6), it is seen that it is 45.3% damping at the resonant frequency amplitude at ζ_1, 68.4% at ζ_2, 86.8% at ζ_3, 93.4% at ζ_4 and 96,8% at ζ_5.

Table 4. Frequency response normal stress maximum amplitudes and phase angles

zeta	Value type	Normal stress x-axis	Normal stress y-axis	Normal stress z-axis
0		39000	39000	39000
0,01	Maximum	39000	39000	39000
0,02	resonant	39000	39000	39000
0,05	frequency	39000	39000	39000
0,1	(Hz)	38000	38000	38000
0,2		37000	38000	37000
0		1,13E-02	3,22E-02	6,84E-02
0,01		6,54E-03	1,87E-02	3,97E-02
0,02	Maximum	3,78E-03	1,08E-02	2,29E-02
0,05	amplitude	1,60E-03	4,52E-03	9,63E-03
0,1		8,49E-04	2,27E-03	4,89E-03
0,2		4,60E-04	1,13E-03	2,47E-03
0		180	180	180
0,01		-124,83	-125,68	-125,49
0,02	Phase	-108,39	-110,09	-109,72
0,05	angle (°)	-95,188	-99,372	-9,84E+01
0,1		-74,632	-81,532	-8,00E+01
0,2		-70,389	-88,576	-7,83E+01
0	Damped	0,00%	0,00%	0,00%
0,01	maximum	-42,02%	-42,05%	-42,04%
0,02	amplitude	-66,45%	-66,51%	-66,50%
0,05	concerning	-85,80%	-85,95%	-85,92%
0,1	zeta = 0	-92,47%	-92,96%	-92,86%
0,2		-95,92%	-96,50%	-96,38%

Table 6. Frequency response normal elastic strain maximum amplitudes and phase angles

zeta	Value type	Normal stress x-axis	Normal stress y-axis	Normal stress z-axis
0		39000	58000	39000
0,01	Maximum	39000	39000	39000
0,02	resonant	39000	39000	39000
0,05	frequency	39000	39000	39000
0,1	(Hz)	39000	39000	38000
0,2		38000	39000	37000
0		8,24E-08	5,80E-08	2,74E-07
0,01		4,78E-08	2,79E-08	1,59E-07
0,02	Maximum	2,76E-08	1,61E-08	9,20E-08
0,05	amplitude	1,16E-08	6,73E-09	3,86E-08
0,1		5,74E-09	3,32E-09	1,96E-08
0,2		2,75E-09	1,55E-09	9,91E-09
0		-9,26E-14	-9,26E-14	180
0,01		53,963	-126,32	-125,5
0,02	Phase	69,195	-111,36	-109,73
0,05	angle (°)	78,855	-102,54	-98,485
0,1		79,991	-102,74	-80,034
0,2		85,476	-107,89	-78,459
0	Damped	0,00%	0,00%	0,00%
0,01	maximum	-42,05%	-51,93%	-42,04%
0,02	amplitude	-66,52%	-72,24%	-66,50%
0,05	concerning	-85,99%	-88,40%	-85,92%
0,1	zeta = 0	-93,04%	-94,27%	-92,86%
0,2		-96,67%	-97,33%	-96,39%

Table 5. Frequency response directional deformation maximum amplitudes and phase angles

zeta	Value type	Normal stress x-axis	Normal stress y-axis	Normal stress z-axis
0		39000	39000	39000
0,01	Maximum	39000	39000	39000
0,02	resonant	39000	39000	39000
0,05	frequency	39000	39000	39000
0,1	(Hz)	38000	38000	39000
0,2		37000	37000	38000
0		6,44E-06	4,89E-02	1,89E-09
0,01		2,16E-06	2,83E-02	6,44E-10
0,02	Maximum	7,24E-07	1,64E-02	2,19E-10
0,05	amplitude	1,28E-07	6,88E-03	4,18E-11
0,1		3,38E-08	3,50E-03	1,29E-11
0,2		9,10E-09	1,79E-03	5,03E-12
0		180	-9,26E-14	-9,26E-14
0,01		-70,012	54,578	104,38
0,02	Phase	-37,495	70,424	131,82
0,05	angle (°)	-12,059	81,904	142,12
0,1		29,292	100,68	135,29
0,2		40,675	102,83	130,91
0	Damped	0,00%	0,00%	0,00%
0,01	maximum	-66,41%	-42,04%	-65,98%
0,02	amplitude	-88,77%	-66,49%	-88,42%
0,05	concerning	-98,01%	-85,92%	-97,79%
0,1	zeta = 0	-99,47%	-92,83%	-99,32%
0,2		-99,86%	-96,35%	-99,73%

4. Conclusions and Recommendations

According to the frequency response data obtained as a result of finite element analysis, a total of three different resonant frequency values were determined, with the largest being 39000 Hz, 58000 and 79000. In the gudgeon pin model used in the internal combustion engine, these frequencies are found at the following rpm engine speed values:

$$39000 \ Hz = 650 \ RPM \qquad (24.1)$$

$$58000 \ Hz = 967 \ RPM \qquad (24.2)$$

$$79000 \ Hz = 1317 \ RPM \qquad (24.3)$$

Idle speed in internal combustion engines is generally set in the range of 600-1000 RPM. If the motor idle speed is set as one of the values of Equation (24.1), (24.2), and (24.3), the stress, strain, and deformation values on the gudgeon pin will be higher than expected due to the resonance that may occur, and the gudgeon pin will be damaged. The resonant frequency can be damped with a damper to prevent or reduce the effects of resonance. In the frequency response graphs in Fig. 6-11, the curves of the damped resonant frequencies at six different zeta (ζ) values are also shown. When the zeta value is 0.2, all resonant frequencies are almost entirely damped.

References

Arioli, G., & Gazzola, F. (2015). A new mathematical explanation of what triggered the catastrophic torsional mode of the Tacoma Narrows Bridge. *Applied Mathematical Modelling*, *39*(2), 901–912.

https://doi.org/https://doi.org/10.1016/j.apm.2014.06.022

Binoy, J., Marchewka, M. K., & Jayakumar, V. S. (2013). The 'partial resonance' of the ring in the NLO crystal melaminium formate: Study using vibrational spectra, DFT, HOMO–LUMO and MESP mapping. *Spectrochimica Acta Part A: Molecular and Biomolecular Spectroscopy*, *104*, 97–109. https://doi.org/https://doi.org/10.1016/j.saa.2012.11.046

Closed-loop random vibration control of a shaker table with a microcomputer: M. L. Wang, Soil Dynamics & Earthquake Engineering, 13(4), 1994, pp 259–266. (1995). *International Journal of Rock Mechanics and Mining Sciences & Geomechanics Abstracts*, *32*(1), A24. https://doi.org/https://doi.org/10.1016/0148-9062(95)90179-5

Diéguez, P. M., Urroz, J. C., Sáinz, D., Machin, J., Arana, M., & Gandía, L. M. (2018). Characterization of combustion anomalies in a hydrogen-fueled 1.4 L commercial spark-ignition engine by means of in-cylinder pressure, block-engine vibration, and acoustic measurements. *Energy Conversion and Management*, *172*, 67–80. https://doi.org/https://doi.org/10.1016/j.enconman.2018.06.115

Fung, R.-F., & Chen, K.-W. (1998). Dynamic Analysis And Vibration Control of A Flexible Slider–Crank Mechanism Using Pin Synchronous Servo Motor Drive. *Journal of Sound and Vibration*, *214*(4), 605–637. https://doi.org/https://doi.org/10.1006/jsvi.1998.1556

Geng, Z., & Chen, J. (2005). Investigation into piston-slap-induced vibration for engine condition simulation and monitoring. *Journal of Sound and Vibration*, *282*(3), 735–751. https://doi.org/https://doi.org/10.1016/j.jsv.2004.03.057

Geng, Z., Chen, J., & Barry Hull, J. (2003). Analysis of engine vibration and design of an applicable diagnosing approach. *International Journal of Mechanical Sciences*, *45*(8), 1391–1410. https://doi.org/https://doi.org/10.1016/j.ijmecsci.2003.09.012

Gharaibeh, M. A., & Pitarresi, J. M. (2019). Random vibration fatigue life analysis of electronic packages by analytical solutions and Taguchi method. *Microelectronics Reliability*, *102*, 113475. https://doi.org/10.1016/j.microrel.2019.113475

Gosala, D. B., Raghukumar, H., Allen, C. M., Shaver, G. M., McCarthy, J. E., & Lutz, T. P. (2021). Model-based design of dynamic firing patterns for supervisory control of diesel engine vibration. *Control Engineering Practice*, *107*, 104681. https://doi.org/https://doi.org/10.1016/j.conengprac.2020.104681

Haftirman, A. K. R. (2016). *Mechanical System Design Lecture Note (Lecture 13) Multicylinder Engines*.

Jannoun, M., Aoues, Y., Pagnacco, E., Pougnet, P., & El-Hami, A. (2017). Probabilistic fatigue damage estimation of embedded electronic solder joints under random vibration. *Microelectronics Reliability*, *78*, 249–257. https://doi.org/10.1016/j.microrel.2017.08.005

Karkoub, M. A. (2000). Control of the elastodynamic vibrations of a flexible slider–crank mechanism using μ-synthesis. *Mechatronics*, *10*(6), 649–668. https://doi.org/https://doi.org/10.1016/S0957-4158(99)00083-5

Kihm, F., & Delaux, D. (2013). Vibration Fatigue and Simulation of Damage on Shaker Table Tests: The Influence of Clipping the Random Drive Signal. *Procedia Engineering*, *66*, 549–564. https://doi.org/https://doi.org/10.1016/j.proeng.2013.12.107

Liao, H. (2014). Global resonance optimization analysis of nonlinear mechanical systems: Application to the uncertainty quantification problems in rotor dynamics. *Communications in Nonlinear Science and Numerical Simulation*, *19*(9), 3323–3345. https://doi.org/https://doi.org/10.1016/j.cnsns.2014.02.026

Liu, X., & Randall, R. B. (2005). Blind source separation of internal combustion engine piston slap from other measured vibration signals. *Mechanical Systems and Signal Processing*, *19*(6), 1196–1208. https://doi.org/https://doi.org/10.1016/j.ymssp.2005.08.004

Malík, J. (2013). Sudden lateral asymmetry and torsional oscillations in the original Tacoma suspension bridge. *Journal of Sound and Vibration*, *332*(15), 3772–3789. https://doi.org/https://doi.org/10.1016/j.jsv.2013.02.011

Matsumoto, M., Shirato, H., Yagi, T., Shijo, R., Eguchi, A., & Tamaki, H. (2003). Effects of aerodynamic interferences between heaving and torsional vibration of bridge decks: the case of Tacoma Narrows Bridge. *Journal of Wind Engineering and Industrial Aerodynamics*, *91*(12), 1547–1557. https://doi.org/https://doi.org/10.1016/j.jweia.2003.09.010

Moosavian, A., Najafi, G., Ghobadian, B., & Mirsalim, M. (2017). The effect of piston scratching fault on the vibration behavior of an IC engine. *Applied Acoustics*, *126*, 91–100. https://doi.org/https://doi.org/10.1016/j.apacoust.2017.05.017

Moosavian, A., Najafi, G., Ghobadian, B., Mirsalim, M., Jafari, S. M., & Sharghi, P. (2016). Piston scuffing fault and its identification in an IC engine by vibration analysis. *Applied Acoustics*, *102*, 40–48. https://doi.org/https://doi.org/10.1016/j.apacoust.2015.09.002

Muhammad, N., Fang, Z., & Shoaib, M. (2020). Remaining useful life (RUL) estimation of electronic solder joints in rugged environment under random vibration. *Microelectronics Reliability*, *107*, 113614. https://doi.org/10.1016/j.microrel.2020.113614

Naseri, R., Talebi, H. A., Ohadi, A., & Fakhari, V. (2020). A robust active control scheme for automotive engine vibration based on disturbance observer. *ISA Transactions*, *100*, 13–27. https://doi.org/https://doi.org/10.1016/j.isatra.2019.11.005

Plaut, R. H. (2008). Snap loads and torsional oscillations of the original Tacoma Narrows Bridge. *Journal of Sound and Vibration*, *309*(3), 613–636. https://doi.org/https://doi.org/10.1016/j.jsv.2007.07.057

Reghu, V. R., Shankar, V., & Ramaswamy, P. (2018). Challenges in Plasma Spraying of 8%Y2O3-ZrO2 Thermal Barrier Coatings on Al Alloy Automotive Piston and Influence of Vibration and Thermal Fatigue on Coating Characteristics. *Materials Today: Proceedings*, *5*(11, Part 3), 23927–23936. https://doi.org/https://doi.org/10.1016/j.matpr.2018.10.185

Strozzi, A., Baldini, A., Giacopini, M., Bertocchi, E., & Mantovani, S. (2018). A repertoire of failures in gudgeon pins for internal combustion engines, and a critical assessment of the design formulae. *Engineering Failure Analysis*, *87*, 22–48. https://doi.org/10.1016/j.engfailanal.2018.02.004

Trapp, A., & Wolfsteiner, P. (2021). Frequency-domain characterization of varying random vibration loading by a non-stationarity matrix. *International Journal of Fatigue*, *146*, 106115. https://doi.org/10.1016/j.ijfatigue.2020.106115

Veciana Fontanet, J. M., Jordi Nebot, L., & Lores Garcia, E. (2021). Residual vibration reduction in back-and-forth moving systems driven by slider-crank mechanisms working through a dead point configuration. *Mechanism and Machine Theory*, *158*, 104239. https://doi.org/https://doi.org/10.1016/j.mechmachtheory.2020.104239

Wang, M. L. (1994). Closed-loop random vibration control of a shaker table with a microcomputer. *Soil Dynamics and Earthquake Engineering*, *13*(4), 259–266. https://doi.org/https://doi.org/10.1016/0267-7261(94)90030-2

Wu, L., Bi, Y., Shen, L., Lei, J., Zhang, L., & Zhou, F. (2019). Study on the effect of piston skirt profile on the vibration behavior of non-road high pressure common rail diesel engine. *Applied Acoustics*, *148*, 457–466. https://doi.org/https://doi.org/10.1016/j.apacoust.2019.01.007

Wyatt, T. A. (1992). Bridge Aerodynamics 50 Years After Tacoma Narrows - Part I: The Tacoma Narrows failure and after. *Journal of Wind Engineering and Industrial Aerodynamics*, *40*(3), 317–326. https://doi.org/https://doi.org/10.1016/S0167-6105(18)80001-0

Xu, X. L., & Yu, Z. W. (2010). Failure investigation of a diesel engine piston pin. *Journal of Failure Analysis and Prevention*, *10*(3), 245–248. https://doi.org/10.1007/s11668-010-9343-x

Yao, G., & Li, F. (2019). Nonlinear global resonance analysis of an embedded plate interacting with outside subsonic airflow. *Communications in Nonlinear Science and Numerical Simulation*, *68*, 286–301. https://doi.org/https://doi.org/10.1016/j.cnsns.2018.08.010

Yu, Z., Xu, X., & Ding, H. (2007). Failure analysis of a diesel engine piston-pin. *Engineering Failure Analysis*, *14*(1), 110–117. https://doi.org/10.1016/j.engfailanal.2005.12.004